ChemComm

ROYAL SOCIETY OF CHEMISTRY

COMMUNICATION

Published on 23 July 2026
Licence and permissions

Check for updates

Cite this: DOI: 10.1039/d6cc04125f

Received 27th June 2026,
Accepted 21st July 2026

DOI: 10.1039/d6cc04125f

rsc.li/chemcomm

Surfactant-mediated reduction at water microdroplet interfaces enables switchable synthesis of silver nanoparticles and ammonia

Sinchan Mukhopadhyay, [a] Depanjan Sarkar *[ab] and Thalappil Pradeep *[abc]

Aqueous microdroplets enable surfactant-mediated macroscopic synthesis of Ag nanoparticles and ammonia under argon and nitrogen, respectively, without external voltage or common reducing agents. Control studies reveal surfactant charge-induced reactivity at aqueous microdroplet interfaces, offering a green route for reduction in confined aqueous environments.

Microdroplets have emerged as versatile platforms for material synthesis and chemical transformations, often enabling unusual reactions that proceed with accelerated kinetics and, in some cases, without added catalysts.[1–13] Their high surface-to-volume ratio, the presence of strong interfacial electric fields of the order of 10^7–10^9 V m^{-1} (in the case of charged microdroplets), and the unique reorganization of molecules and ions at the air–water interface (AWI) underpin their distinctive physicochemical behaviour.[14–22] Oxidation reactions have been the major focus in microdroplet chemistry, due to the abundant formation of water radical cations, hydroxyl radicals, hydrogen peroxide and singlet oxygen[23] at the interface, arising from enhanced auto-ionization and electron detachment processes under the high interfacial electric field. By contrast, reduction reactions at microdroplet interfaces have been explored to a much lesser extent. One such example is a recent report on the reduction of the carbonyl groups to alcohols at the AWI.[24] On the other hand, microdroplets have been shown to reduce metal ions to nanoparticles, driven by interfacial electric fields.[25–27] Moreover, N_2, one of the most abundant yet chemically inert molecules in the atmosphere, has recently been reduced to NH_3 and related molecules in water microdroplets through both catalytic and catalyst-free pathways.[28–30]

Here, we demonstrate that sodium dodecyl sulphate (SDS), an anionic surfactant, can cause enhanced reduction chemistry in water microdroplets generated *via* ultrasonic nebulization alone, with no applied voltage. Using Ag^+ reduction as a model reaction, we find that SDS-containing microdroplets produce silver nanoparticles (Ag NPs) on a macroscopic scale at a much faster rate under an Ar atmosphere, without any external voltage or reducing agents. When the same SDS-containing microdroplet system was operated under a N_2 atmosphere, NH_3 was formed, indicating that the surfactant-modified interface promoted N_2 reduction under apparently mild conditions. In contrast to earlier microdroplet methods,[10,26,27] our approach demonstrates that molecular assembly at interfaces alone can drive programmable macroscopic synthesis. Together, these results suggest that surfactant-controlled interfacial organization can be used to enhance reduction and enable reduction reactions in microdroplet environments.

Fig. 1 illustrates the reaction setup and the process. Microdroplets were generated in a glass vessel containing an aqueous solution of the reagents using a commercial ultrasonic mist generator (see S1 for a detailed description). The mist generator was placed in a thermostated water bath, and the reaction vessel was positioned above it. During operation, the ultrasonic nebulizer produced a continuous plume of microdroplets within the reaction chamber. At the end of the reaction, it was switched off, allowing the microdroplets to coalesce and settle into the bulk solution. The bulk solution was collected and characterised. The temperature of the reaction medium was maintained constant throughout, and the gaseous atmosphere (argon, nitrogen, or, air) within the vessel was adjusted for various experiments.

To start with, a 10 ml mixture of 1 mM $AgNO_3$ and 1 mM SDS was added into the reaction vessel and subjected to ultrasonic nebulization for 1 h in ambient conditions. Upon completion, the bulk part was analysed by UV-visible spectroscopy. No colour change was observed, and the spectrum showed no surface plasmon resonance (SPR) band characteristic of Ag NPs (Fig. 2A). Here, O_2 may act as an electron scavenger

[a] DST Unit of Nanoscience (DST UNS) & Thematic Unit of Excellence (TUE), Department of Chemistry, Indian Institute of Technology Madras (IITM), Chennai-600036, India. E-mail: depanjansarkar@gmail.com, pradeep@iitm.ac.in
[b] Centre of Excellence on Molecular Materials and Functions, Department of Chemistry, Indian Institute of Technology Madras, Chennai-600036, India
[c] International Centre for Clean Water, IIT Madras Research Park, 2nd Floor, B-Block, Kanagam Road, Taramani, Chennai-600113, India

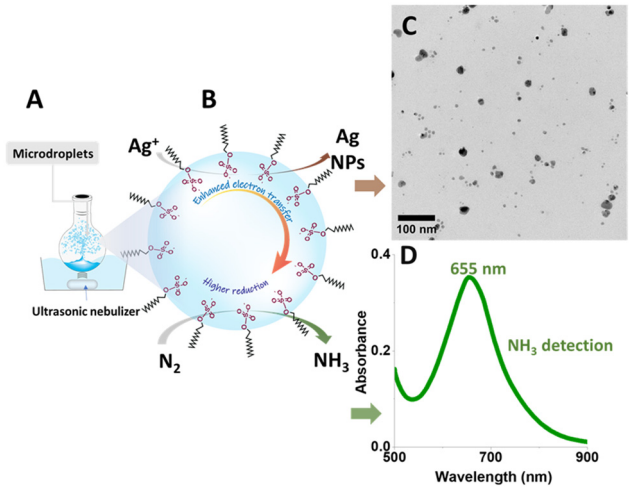

Fig. 1 (A) Schematic of the experimental setup, (B) enhanced reduction at the air–water interface of SDS-containing microdroplets. Analysis showing that (C) Ag^+ ions are reduced to metallic Ag nanoparticles (a large-area TEM image) and (D) N_2 is converted to NH_3, as evidenced by the UV-vis spectrum obtained using the modified Berthelot method.

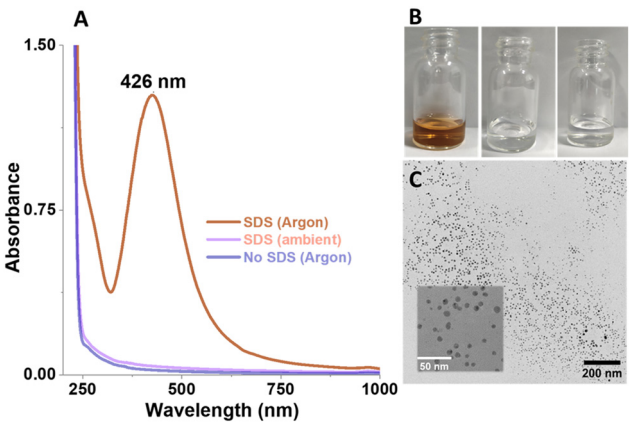

Fig. 2 (A) UV-visible spectra of the reaction medium of Ag^+ after microdroplet reactions under different conditions: SDS (Ar), SDS (ambient), and no SDS (Ar). (B) Corresponding photographs of the solutions [left to right: SDS (Ar), SDS (ambient), and no SDS (Ar)]. (C) Large-area TEM image of Ag nanoparticles formed in SDS (Ar).

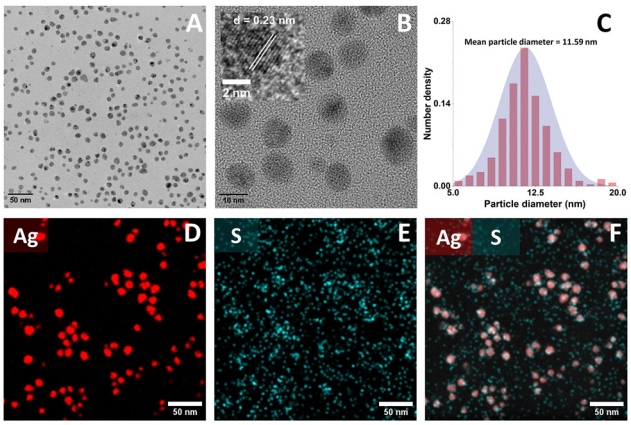

Fig. 3 TEM images of Ag NPs generated in a SDS-containing reaction medium under argon: (A) and (B) TEM images at different magnifications, with the inset showing the lattice fringes; (C) particle size distribution obtained from the TEM image; and (D)–(F) HAADF-STEM images showing the presence of Ag and S (from the sulphate group of SDS) and their overlay. SDS is present all over the grid as expected.

$(O_2 + e^- \rightarrow O_2^{-\bullet})$, intercepting interfacial electrons before they could reduce Ag^+. To test this, dissolved gases were removed from the solution by purging and filling with Ar prior to nebulization. After the experiment, the resulting solution turned reddish-brown (Fig. 2B), and the UV-vis spectrum showed a distinct SPR peak at 426 nm, confirming the formation of Ag NPs. Large-area TEM imaging (Fig. 2C) of this solution formed under Ar + SDS conditions confirms the presence of Ag NPs, consistent with the SPR peak. In a control experiment without SDS (1 mM $AgNO_3$ only, under Ar), no colour change occurred and no SPR peak was detected (Fig. 2A), demonstrating that SDS was essential for enabling interfacial electron transfer and Ag^+ reduction in microdroplets. Without SDS, the neutral interface lacks organised negative charges arising from sulphate headgroups, and electrons did not accumulate effectively even under inert conditions. Varying the SDS concentration relative to $AgNO_3$ significantly modulates the NP population and size. An increase in SDS up to 5-fold enhances the reduction, as evidenced by a higher population of Ag NPs (Fig. S1). Concurrently, the SPR band exhibits a red-shift, indicating larger particle sizes. At higher concentrations (1 : 10 ratio, >8 mM, above the critical micellar concentration, CMC), the SPR band broadens and shifts to 465 nm with decreased intensity, consistent with the formation of larger, more polydisperse NPs that effectively limit further growth and reduce the total NP population. To further elucidate the reduction dynamics, a time-dependent study was conducted (Fig. S2). This analysis confirms the accelerated formation of Ag NPs in the presence of SDS, providing quantitative insight into the enhanced interfacial reduction kinetics. These spectral trends are corroborated by TEM images of Ag NPs at various $AgNO_3$: SDS ratios (Fig. 3 and Fig. S3).

The synthesized Ag NPs were further characterised using transmission electron microscopy (TEM) and scanning transmission electron microscopy (STEM), as shown in Fig. 3. The TEM image (Fig. 3A) reveals predominantly near-spherical NPs. A high-resolution TEM image (Fig. 3B) shows clear lattice fringes with an interplanar spacing of 0.23 nm (inset), corresponding to the (111) plane of metallic Ag, confirming their crystalline nature. Selected area electron diffraction (SAED) analysis (Fig. S4) also confirms the crystalline nature of the NPs. The particle size distribution (Fig. 3C) indicates an average diameter of 11.59 nm calculated using ImageJ software from a collection of 266 particles (see experimental details). High-angle annular dark-field (HAADF) STEM and elemental mapping reveal the presence of both Ag and S, with Ag localized in the nanoparticle cores and S distributed around the particles (Fig. 3D–F). The sulphur signal originates from the sulphate

 This journal is © The Royal Society of Chemistry 2026

head groups of SDS, indicating that the surfactant protects the nanoparticle surface, preventing the aggregation of nanoparticles.

To assess the surfactant's ionic nature on Ag NP formation, CTAN and Triton X-100 were also examined (Fig. S5). In the UV-vis spectrum, both shows broader peaks centred at ~435 nm and ~465 nm, respectively, with markedly lower intensity and with no pronounced plasmon peaks, indicating reduced Ag NP formation. These observations suggest that the −ve charged sulfate head groups of SDS possibly enhance the interfacial negative charge and promote reduction, than cationic and non-ionic surfactants.

To probe the mechanism, charges of the droplets formed were examined using a Faraday cup. SDS- and CTAB-containing microdroplets exhibited −ve and +ve charges, respectively, whereas Triton X-100 and water produced weaker −ve and +ve charges, respectively (Fig. S6A). Increasing the SDS concentration led to progressively more −ve charged droplets (Fig. S6B). We conclude that SDS promotes a −ve charged interfacial environment, which may facilitate reduction processes at the AWI.

For gaining mechanistic insights, the solution was analysed by mass spectrometry before and after nebulization. Several oxidation-derived species of SDS (*m*/*z* 263, 279, 283, and 297) were observed only after nebulization, indicating oxidative transformation of the dodecyl chain (Fig. S7A and B). Collision-induced dissociation (CID) analysis of these species showed fragmentation of the oxidized alkyl chain along with the formation of the bisulphate ion (Fig. S8). Similar characteristic fragmentation was observed for SDS, suggesting that the oxidized products originate from SDS. These results indicate that SDS undergoes oxidation during nebulization and may act as a sacrificial agent responsible for the observed reduction reaction.

So far, our results demonstrate enhanced reduction in SDS-containing microdroplets under an inert atmosphere. To extend this study, we explored the reduction of N_2 to NH_3, a chemically demanding process due to the strong N≡N bond. Researchers have already demonstrated that water microdroplets can facilitate the conversion of N_2 into NH_3 and other nitrogen-containing species using an $^{15}N_2$ isotopic labelling study.[30] Here, we focused majorly on the effect on NH_3 formation in surfactant-containing microdroplets. An aqueous SDS solution was thoroughly deoxygenated and purged with high-purity N_2, followed by nebulization for 4 h. The collected solution was analysed for NH_3 using a modified Berthelot method (see the SI), monitored *via* UV-vis spectroscopy. A characteristic peak at 655 nm confirmed NH_3 formation, which was quantified using a calibration curve constructed from standard NH_3 solutions (Fig. S9A and B). Notably, increased NH_3 formation was observed in the absence of Ag^+ ions. However, upon addition of Ag^+ along with SDS, NH_3 production was significantly suppressed (Fig. 4A).

Then, the extent of NH_3 formation was evaluated through a series of control experiments (Fig. 4B and Fig. S10). Unless otherwise stated, no Ag^+ ions were used in these experiments. A control experiment (standard NH_3 ± SDS) showed almost no change in absorbance, showing that SDS present in the reaction

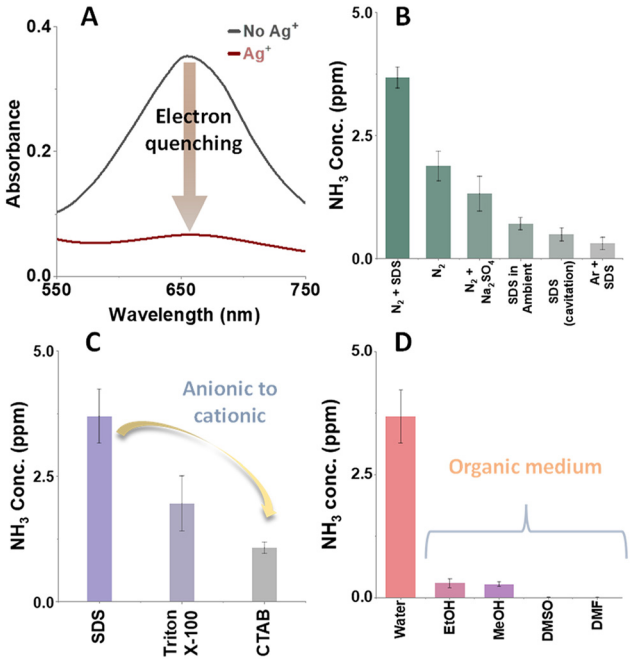

Fig. 4 UV-vis spectra using the modified Berthelot method for NH_3 detection: (A) NH_3 formation in the presence and absence of Ag^+ ions, showing competition for reduction; (B) NH_3 formation under different reaction environments; (C) NH_3 production with SDS, Triton X-100, and CTAB; and (D) NH_3 production under different solvents.

mixture does not interfere with the modified Berthelot's method (Fig. S11). Control experiments were also performed to exclude possible contamination of NH_3 from external factors (Fig. S12). In the absence of SDS, even under an N_2 atmosphere, only a small amount of NH_3 was detected, highlighting the critical role of the surfactant in facilitating the reaction. In contrast, when the reaction was performed under ambient conditions, NH_3 formation was significantly suppressed despite the presence of SDS. This reduction in activity is attributed to dissolved O_2, which competes for e^- and acts as an e^- scavenger, thereby inhibiting N_2 reduction. Replacement of SDS with an equivalent amount of Na_2SO_4 resulted in a slight decrease in NH_3 formation, likely due to the increased surface tension and larger droplet size (Fig. S13A and B) compared to water alone (Fig. S13C and D). SDS, being a surfactant, can lower surface tension and generate smaller droplets, further elevating the overall surface-to-volume ratio (Fig. S13E and F). The contribution of acoustic cavitation was also examined and it produced negligible NH_3, indicating a minimal role of it. This finding underscores the dominant role of the AWI in driving N_2 reduction. While direct, real-time measurements of electron transfer at the single-droplet level remain a technical challenge, our results are consistent with a possible mechanism involving sacrificial oxidation of SDS and enhanced interfacial negative charge, regulated by a surfactant-modified environment. To further validate the role of N_2, the reaction environment was purged with Ar. Here, NH_3 formation was negligible. Trace amounts could arise from residual N_2, which is experimentally difficult to eliminate completely. While consistent

with microdroplet-assisted NH_3 formation under N_2, definitive assignment of the nitrogen source requires $^{15}N_2$ labelling experiments, as has been reported in a related context.[30]

To probe surfactant effects on NH_3 formation, CTAB and Triton X-100 were examined in place of SDS (Fig. 4C). NH_3 formation followed the order SDS > Triton X-100 (no interference with the Berthelot assay[31]) > CTAB, indicating that negatively charged sulfate head groups promote reduction, whereas positively charged CTAB suppresses it. In contrast, the non-ionic Triton X-100 shows a comparatively minimal effect on the reduction process.

N_2 conversion to NH_3 is expected to proceed through the combined contributions of hydrogen addition and e^- transfer.[30] To investigate this, the reaction medium was systematically varied by replacing water with other polar solvents, including both protic and aprotic systems (Fig. 4D). In methanol and ethanol, only minimal NH_3 formation was observed compared to that in water, due to the lower extent of H radical generation from these solvents. For other polar aprotic solvents such as dimethyl sulfoxide (DMSO) and *N*,*N*-dimethylformamide (DMF), NH_3 formation was negligible, consistent with the extremely limited generation of hydrogen radicals. In addition, e^- transfer also plays a critical role in N_2 reduction and is strongly influenced by the dielectric constant and conductivity of the solvent. Water, with its higher dielectric constant and conductivity, relative to the other solvents studied, facilitates more efficient electron transfer, thereby leading to enhanced NH_3 formation.

In conclusion, we demonstrate that surfactant-organized microdroplets generated *via* ultrasonic nebulization drive both Ag^+ reduction to crystalline NPs and N_2-to-NH_3 conversion, without external reductants. Droplet charge measurements support that SDS enhances interfacial reduction by increasing the negative charge density at the AWI. Also, SDS acts as a sacrificial agent to promote enhanced reduction, demonstrated using mass spectrometric analysis. Control experiments further reveal that the microdroplet redox activity is governed by interfacial charge, solvent polarity, and competitive electron scavenging by O_2. These findings establish that the surfactant head-group chemistry, solvent properties, and gaseous environment cooperatively regulate electron transfer at the AWI, providing a framework for tuning microdroplet reactivity. This surfactant-mediated interfacial organization opens new avenues for sustainable reduction chemistry in confined environments, with potential applications extending beyond Ag NP synthesis and nitrogen fixation to interfacial catalysis.

Conflicts of interest

There are no conflicts to declare.

Data availability

The data supporting this article have been included in the supplementary information (SI). Supplementary information is available. See DOI: https://doi.org/10.1039/d6cc04125f.

Acknowledgements

This work was supported by the ANRF Science and Engineering Research Board (SERB), Department of Science and Technology (DST), Government of India. T. P. acknowledges support from SERB under the SUPRA scheme (SPR/2021/000439) and a JC Bose Fellowship. We acknowledge the support of the Centre of Excellence on Molecular Materials and Functions under the Institution of Eminence Scheme of IIT Madras. TEM measurements were performed at the ANRF SERB National Facility for Cryo-Electron Microscopy, IIT Madras. S. M. also acknowledges CSIR-UGC for his fellowship.

References

1 B. K. Spoorthi, K. Debnath, P. Basuri, A. Nagar, U. V. Waghmare and T. Pradeep, *Science*, 2024, **384**, 1012–1017.
2 A. Ray Chowdhuri, B. K. Spoorthi, B. Mondal, P. Bose, S. Bose and T. Pradeep, *Chem. Sci.*, 2021, **12**, 6370–6377.
3 A. Mahapatra, A. Som, B. K. Spoorthi, D. Sarkar and T. Pradeep, *Chem. Commun.*, 2025, **61**, 15846–15849.
4 T. Pradeep, *ACS Sustainable Chem. Eng.*, 2026, **14**, 25–30.
5 M. Girod, E. Moyano, D. I. Campbell and R. G. Cooks, *Chem. Sci.*, 2011, **2**, 501–510.
6 J. K. Lee, S. Kim, H. G. Nam and R. N. Zare, *Proc. Natl. Acad. Sci. U. S. A.*, 2015, **112**, 3898–3903.
7 J. K. Lee, S. Banerjee, H. G. Nam and R. N. Zare, *Q. Rev. Biophys.*, 2015, **48**, 437–444.
8 J. K. Lee, D. Samanta, H. G. Nam and R. N. Zare, *Nat. Commun.*, 2018, **9**, 1562.
9 A. Li, Q. Luo, S. Park and R. G. Cooks, *Angew. Chem., Int. Ed.*, 2014, **53**, 3147–3150.
10 D. Sarkar, M. K. Mahitha, A. Som, A. Li, M. Wleklinski, R. G. Cooks and T. Pradeep, *Adv. Mater.*, 2016, **28**, 2223–2228.
11 Z. Wei, Y. Li, R. G. Cooks and X. Yan, *Annu. Rev. Phys. Chem.*, 2020, **71**, 31–51.
12 J. Ghosh and R. G. Cooks, *TrAC, Trends Anal. Chem.*, 2023, **161**, 117010.
13 P. Basuri, S. Mukhopadhyay, K. S. S. V. P. Reddy, K. Unni, B. K. Spoorthi, J. Shantha Kumar, S. S. R. K. C. Yamijala and T. Pradeep, *Angew. Chem., Int. Ed.*, 2024, **63**, e202403229.
14 K. R. Wilson and A. M. Prophet, *Annu. Rev. Phys. Chem.*, 2024, **75**, 185–208.
15 H. Xiong, J. K. Lee, R. N. Zare and W. Min, *J. Phys. Chem. Lett.*, 2020, **11**, 7423–7428.
16 H. Xiong, J. K. Lee, R. N. Zare and W. Min, *J. Phys. Chem. B*, 2020, **124**, 9938–9944.
17 H. Hao, I. Leven and T. Head-Gordon, *Nat. Commun.*, 2022, **13**, 280.
18 S. Lin, L. N. Y. Cao, Z. Tang and Z. L. Wang, *Proc. Natl. Acad. Sci. U. S. A.*, 2023, **120**, e2307977120.
19 K. Gong, J. Ao, K. Li, L. Liu, Y. Liu, G. Xu, T. Wang, H. Cheng, Z. Wang, X. Zhang, H. Wei, C. George, A. Mellouki, H. Herrmann, L. Wang, J. Chen, M. Ji, L. Zhang and J. S. Francisco, *Proc. Natl. Acad. Sci. U. S. A.*, 2023, **120**, e2219588120.
20 K. J. Vannoy, M. Q. Edwards, C. Renault and J. E. Dick, *Annu. Rev. Anal. Chem.*, 2024, **17**, 149–171.
21 K. Lee, M. A. Mehrgardi and R. N. Zare, *J. Am. Chem. Soc.*, 2025, **147**, 33240–33247.
22 D. T. Holden, B. A. Shira, M. Q. Edwards, N. M. Morato and R. G. Cooks, *Chem. Sci.*, 2025, **16**, 17020–17033.
23 F. Li, J. Lv, A. He, J. Xu, L. Zhao, X. Wang, L. Mao, S. Li, H. Wang, Y. Wang and G. Jiang, *J. Am. Chem. Soc.*, 2025, **147**, 30574–30581.
24 J. K. Lee, D. Samanta, H. G. Nam and R. N. Zare, *J. Am. Chem. Soc.*, 2019, **141**, 10585–10589.
25 D. Sarkar, R. Singh, A. Som, C. K. Manju, M. A. Ganayee, R. Adhikari and T. Pradeep, *J. Phys. Chem. C*, 2018, **122**, 17777–17783.
26 S. Bose and R. N. Zare, *Chem. Sci.*, 2025, **16**, 15455–15461.

 This journal is © The Royal Society of Chemistry 2026

27 J. Zhang, C. Zhu and X. Zhang, *J. Am. Chem. Soc.*, 2026, **148**, 4722–4728.
28 X. Song, C. Basheer and R. N. Zare, *Proc. Natl. Acad. Sci. U. S. A.*, 2023, **120**, e2301206120.
29 S. Ma, B. Sui, H. Yuan, A. Yu, G. Chai, S. Zhang, H. Zhang, S. Sun and W. Zhao, *Angew. Chem., Int. Ed.*, 2026, **65**, e24389.
30 Y. Wang, J. Luo, Y.-G. Fang, Z.-A. Nan, X. Cui, T. Chen, X. Zeng, X. Wang, X. Song, J. Zhao, W. Li, C. Zeng, D. Chen, C. Zhu, Z. Wei, Z.-Q. Tian and F. R. Fan, *J. Am. Chem. Soc.*, 2025, **147**, 2756–2765.
31 T. T. Ngo, A. P. H. Phan, C. F. Yam and H. M. Lenhoff, *Anal. Chem.*, 1982, **54**, 46–49.

This journal is © The Royal Society of Chemistry 2026